Dalton Transactions

ROYAL SOCIETY OF CHEMISTRY

PAPER

View Article Online
View Journal | View Issue

Cite this: *Dalton Trans.*, 2024, **53**, 18494

Green synthesis of ZnO-NPs using sugarcane bagasse waste: phytochemical assessment of extract and biological study of nanoparticles†

Marwa H. Suleiman,[a] Said M. El-sheikh, *[b] Eslam T. Mohamed,[c] Mohamed A. El Raey,[d] Samya El Sherbiny,[a] Fatma A. Morsy,[a] Soliman I. El-Hout [b] and Sheta M. Sheta *[e]

The accumulation of agricultural and industrial residues inevitably contributes to environmental pollution. Thus, several scientific investigations have been conducted to overcome this problem and to add an economic value proposition. Unlike typical sugarcane bagasse applications, this work presents a novel application of sugarcane bagasse waste in a green synthesis approach for forming zinc oxide nanoparticles (ZnO-NPs). This work opens the door to studying the potential of sugarcane bagasse in a green synthesis orientation. Phytochemical assessment of the aqueous extract of sugarcane bagasse waste was conducted by studying total flavonoid content, total phenolic content, and antioxidant assays. ZnO-NPs were synthesized using the aqueous sugarcane bagasse extract (ASCBE) with a 96% yield. To obtain 99.7% pure ZnO-NPs, nanoparticles were calcined at 550 °C to remove any remaining plant extract residues. The purity and yield of the produced and modified ZnO-NPs were studied. The initially produced and modified ZnO-NPs were characterized using XRD, FT-IR, UV, TEM, TGA, and PL and to determine the necessity of the calcination step. A detailed proposed mechanism for the formation of ZnO-NPs mediated by ASCBE was introduced. The ZnO-NPs were studied for their antibacterial, antifungal, and antiviral activities. The ZnO-NPs before calcination were found to exhibit more potent antimicrobial activity against both *P. aeruginosa* and *A. niger* compared to the calcined ZnO-NPs. In addition, molecular docking analysis revealed that the ZnO-NPs had the strongest binding affinity towards the *P. aeruginosa* RhlG/NADP active-site complex and the crystal structure of Actibind, a T2 RNase of *A. Niger*. ZnO-NPs also showed promising binding interactions with viral targets, including the Herpes simplex virus type II protease and Influenza virus NS1 effector domain. Additionally, environmental and economic studies were achieved to relate the scientific study with daily life applications.

Received 28th August 2024,
Accepted 15th October 2024

DOI: 10.1039/d4dt02449d

rsc.li/dalton

Introduction

The wonder of modern medicine is a name that nanomaterials have earned through the years because of their remarkable catalytic,[1] optical,[2] antimicrobial,[3] wound healing,[4] and anti-inflammatory properties.[5] Nanomaterials are of considerable interest for investigation in various fields such as medicine,[6] agriculture,[7] environmental remediation,[8] energy storage,[9] electronics,[10] cosmetics,[11] water treatment,[12] and textile manufacturing.[13] Metal oxide nanoparticles are nanomaterials that exhibit impressive physical, chemical, and biological features, making them promising materials for various applications. The fabrication of nanomaterials and metal oxide nanoparticles is explicitly accompanied not only by obstacles related to energy, cost, time, toxic chemical usage, and hazardous waste, but also the stabilization of the nanoparticles; oxidation and agglomeration are serious problems during the synthesis process of nanoparticles.[14] In a world of infectious diseases and epidemics, finding solutions to biological risks is not a luxury for the scientific society but an absolute duty. The fabrication of materials with biological activity will give humanity an advantage in the fight against biological risks.[15–17]

[a]*Department of Chemistry, Faculty of Science, Helwan University, Cairo, 11795, Egypt*
[b]*Department of Nanomaterials and Nanotechnology, Central Metallurgical R & D Institute, Cairo, 11421, Egypt. E-mail: selsheikh2001@gmail.com; Tel: +201022316076*
[c]*Botany and Microbiology Department, Faculty of Science, Helwan University, Ain Helwan, Cairo 11795, Egypt*
[d]*Phytochemistry and Plant Systematics Department, Pharmaceutical And therapeutical Research Industries Institute, National Research Centre, 12622, Egypt*
[e]*Department of Inorganic Chemistry, National Research Centre, Cairo, 12622, Egypt. E-mail: dr.sheta.nrc@gmail.com; Fax: +2-02-33370931; Tel: +201009697356*
† Electronic supplementary information (ESI) available. See DOI: https://doi.org/10.1039/d4dt02449d

Green synthesis techniques for the fabrication of nanomaterials are an excellent alternative solution to the potential difficulties that come with using traditional chemical and physical techniques.[18] Reduced cost,[19] reduced hazardous waste generation,[20] environmental safety,[21] scalability,[22] low chemical and energy consumption,[23] non-toxicity,[24] industrial scalability,[22] and time savings[25] are great benefits that come with the usage of green synthesis techniques. Involving natural extracts in green synthesis has solved the problems of oxidation, stabilization, and agglomeration in traditional techniques due to their role as reductant, antioxidant, capping, and stabilizing agents. Moreover, green synthesis can produce unique shapes of nanoparticles with different sizes and surface features customized for amazing applications.[26,27]

Zinc oxide nanoparticles (ZnO-NPs) are one of the three most-produced nanomaterials, along with silicon and titanium dioxide nanoparticles, due to their various and wide applications.[28,29] ZnO-NPs are critical technological materials due to their outstanding characteristics. The rubber industry,[30] fertilizers,[31] paints,[32] paper coatings,[33] solar cells,[34] microwave absorbers,[35] piezoelectric devices,[36] biomedicines,[37] biosensors,[38] gas sensors,[36] semiconductors,[39] and light-emitting diodes (LED)[40] are examples of industrial applications of ZnO-NPs. Zinc oxide nanoparticles are also reported to have antimicrobial activity, antidiabetic activity, anticancer activity, and drug delivery applications.[41] Like all nanomaterials, ZnO-NPs present manufacturing issues when prepared through traditional methods, which makes the green synthesis of ZnO-NPs using natural extracts an alternative way for traditional ones. Based on previous publications, ZnO-NPs have been effectively synthesized using several natural extracts such as *Aloe vera*,[42] *Passiflora caerulea*,[43] *Azadirachta indica*,[44] and others. ZnO-NPs produced using various extracts demonstrate antibacterial, antioxidant, antifungal, and antiviral properties.

On the other hand, the energy crisis, which is associated with the continuous massive consumption of energy and the constant need to either produce it or create ways to save it, has become one of the world's most challenging issues.[45] Solid waste of various types, *e.g.*, plant, industrial, *etc.*, represents one of the biggest challenges facing our world in the past and present. Therefore, developing plans and strategies to eliminate it and reduce its volume safely for the environment and living organisms is essential. It is essential to discuss and find solutions to both the problems of energy and solid waste.[46] The green transition approach has a high potential to solve problems associated with both energy consumption and waste disposal.[47]

Sugarcane bagasse is the major sugarcane industry by-product (waste). It contains about 50% cellulose, 25% hemicellulose, and 25% lignin.[48] It was employed in energy and many environmental sustainability applications. The annual sugarcane production globally is about 1.60 billion tons, producing about 279.0 million metric tons of sugarcane bagasse waste.[49] Because of all these produced tons, it had to grab the attention of the whole world, especially scientific society, which was employed in many applications. Bagasse is a sustainable and environmentally friendly material source, meeting part of the world's needs for wood in paper manufacturing and biofuel. Scientists have turned their attention to sugarcane bagasse extracts in manufacturing nanomaterials; however, they are not used that much and are expected to have great potential.[50]

To the best of our knowledge, this study aims to synthesize ZnO-NPs using sugarcane bagasse for the first time. A green approach is applied not only for the synthesis method or minimization of solid waste attributed to sugarcane bagasse, but also to contribute to studying the possible energy consumption in the calcination step through a series of comparisons between the properties of the synthesized ZnO-NPs before and after the calcination step. The ZnO-NPs were characterized using XRD, UV, FT-IR, TEM, TGA, and PL. Additionally, a phytochemical assessment of aqueous sugarcane bagasse extract (ASCBE) and a comprehensive evaluation of biological activity including antibacterial, antifungal, and antiviral activity for both ZnO-NP samples were investigated. A detailed proposed mechanism for the formation of ZnO-NPs mediated by ASCBE is presented. An economic and environmental study is discussed to determine the cost of using this proposed methodology for the preparation of ZnO-NPs and the benefits to society.

Results and discussion

The sugarcane bagasse extract was prepared from sugarcane bagasse waste as described in the experimental section and Fig. 1. The phytochemical evaluation as well as the application are discussed in detail as follows:

Phytochemical assessments of ASCBE

The phytochemical analysis helps in identifying the components of plant extracts and understanding the role and behavior of ASCBE in the synthesis of ZnO-NPs. The antioxidant activity, total phenolic content (TPC), and total flavonoid content (TFC) of ASCBE were investigated to determine the possible formation mechanism.

TPC and TFC

The TPC of ASCBE, expressed as gallic acid equivalent, was 12.8 ± 1.1 mg GAE per g extract. TFC, described as rutin equivalent, was 0.6 ± 0.05 mg RE per g extract, as shown in Table 1. The presence of phenolics and flavonoids in ASCBE contributes to its significant antioxidant potential, which makes it suitable for the intended application.

Antioxidant activity

Antioxidant activity was evaluated using 2,2-diphenyl-1-picrylhydrazyl (DPPH), ferric ion reducing antioxidant power (FRAP), and ABTS assays, with results expressed as millimoles of Trolox equivalent per gram (TE g^{-1}) of the sample. The analysis yielded 9.1 ± 0.1 mM TE g^{-1} for DPPH, 163.3 ± 6.8 mM TE g^{-1} for FRAP, and 107.8 ± 2.3 mM TE g^{-1} for ABTS, as

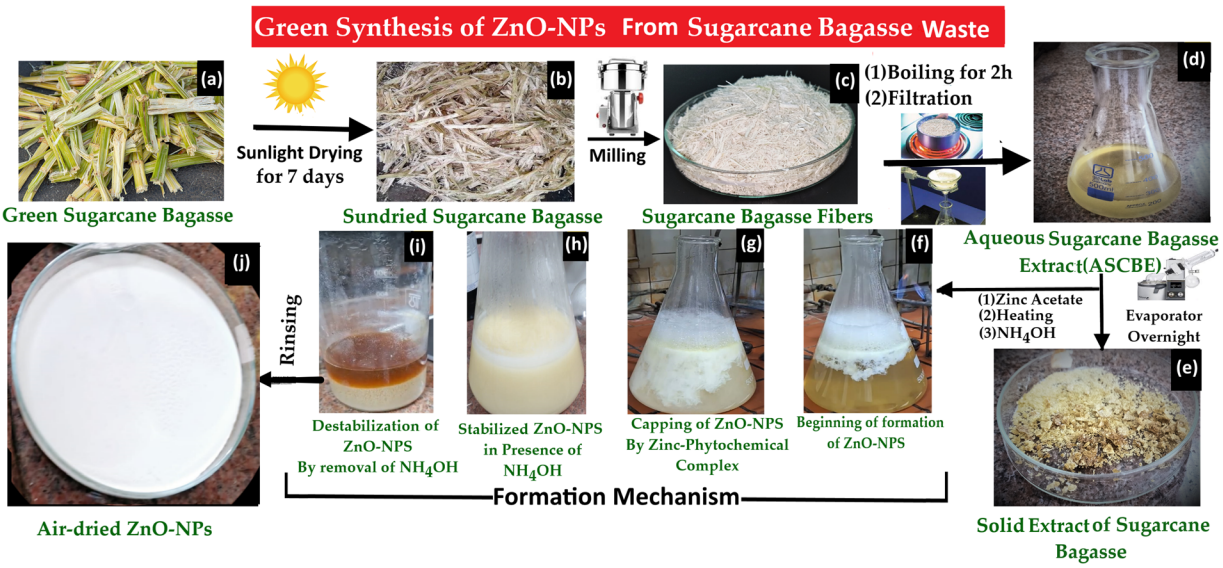

Fig. 1 Scheme of green synthesis of sugarcane bagasse extract and ZnO-NPs from sugarcane bagasse waste and mechanism.

Table 1 Results of TPC, TFC, DPPH, FRAP and ABTS analysis of ASCBE

TPC mg GAE per g of extract	TFC mg RE per g of extract	DPPH mM TE g^{-1} sample	FRAP	ABTS
12.8 ± 1.1	0.6 ± 0.05	9.1 ± 0.1	163.3 ± 6.8	107.8 ± 2.3

shown in Table 1. These findings demonstrate the significant antioxidant activity of ASCBE, which plays a crucial role in reducing the zinc precursor during the nanoparticle formation mechanism that will be discussed later.

Structural and morphological characterization of ZnO-NPs

XRD analysis. Fig. 2a illustrates the XRD spectra for the green-synthesized ZnO-NPs before and after calcination (ZnO-BC and ZnO-AC). The XRD pattern of ZnO-BC exhibits diffraction peaks at 2θ = 31.8°, 34.5°, 36.3°, 47.6°, 56.6° and 62.9°. ZnO-AC displays diffraction peaks at 2θ values of 31.9°, 34.5°, 36.3°, 47.6°, 56.7° and 63.0°. The diffraction peaks of both samples are coincidental to the (100), (002), (101), (102), (110), and (103) diffraction planes. All the diffraction peaks in ZnO-BC and ZnO-AC are ascribed to the crystal structure of the zincite phase (ZnO, JCPDS No. 01-070-2551).[51] The ZnO-NPs conserved their crystal structure after the calcination step, since there was no phase change in either sample. The sharp-

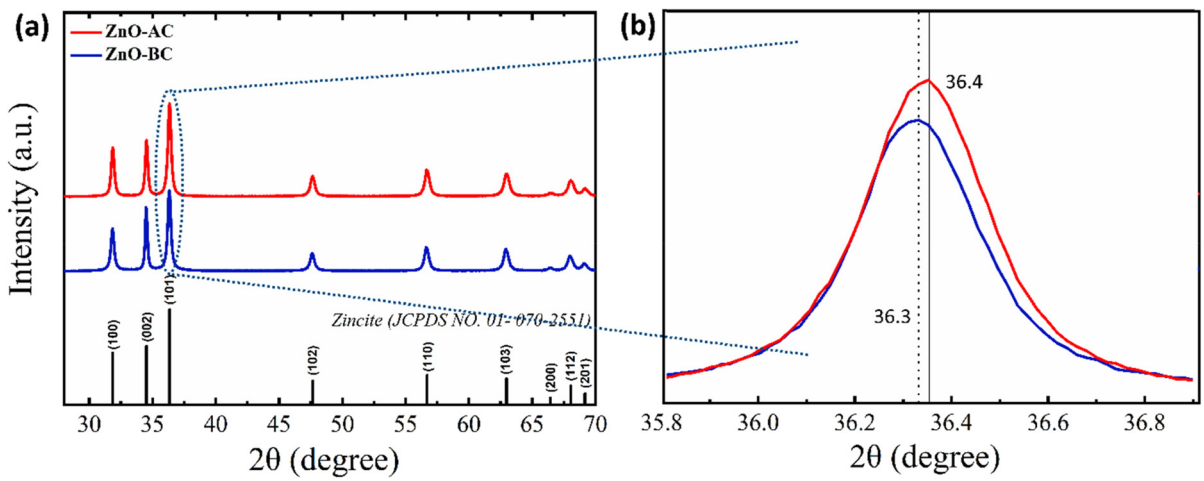

Fig. 2 (a) XRD patterns for ZnO-BC and ZnO-AC, and (b) magnification of the (101) peak.

ness of the peaks in the XRD spectra of both samples indicate a high crystallinity in the prepared ZnO-NPs, but as demonstrated in Fig. 2b, the peak intensity for ZnO-AC at the same angle is higher than that of ZnO-BC, which is evidence for the purity of ZnO-AC as a result of phytochemical removal. Fig. 2b shows that ZnO-AC is exactly coincident with the standard card, but ZnO-BC has a lower 2θ angle shifted about 0.019° due to the presence of sugarcane bagasse extract.

TEM. Fig. 3a and b illustrate the transmission electron microscopy (TEM) images of ZnO-BC and ZnO-AC, respectively. As shown in Fig. 3a, ZnO-BC had hexagonal disk-like structures with diameters ranging from 5 to 30 nm. ZnO-AC (Fig. 3b) had a hexagonal one-dimensional plate-like structure, a diameter of about 20 nm and lengths of about 100 nm with an aspect ratio of about 0.2. The TEM images indicate a high degree of crystallinity within the territories of the nanostructured oxide. The light spots in the TEM images indicate single nanoparticles, while the darker ones correspond to aggregation. However, the obvious accumulation after the calcination step of ZnO-AC-NPs is attributed to the removal of ASCBE, which acts as a capping agent to create voids over and between the nanoparticles, forcing them to stick to one another. Fig. 3c shows a SAED image of ZnO-BC, which reveals that ZnO-BC has a crystalline structure. Moreover, the SAED image is in good agreement with the XRD spectra in Fig. 2a due to all the planes (100), (002), (101) and (102) appearing, which confirms the presence of ZnO-NPs. Fig. 3d shows a SAED image of ZnO-AC, which proves the one-dimensional nanostructure of ZnO-AC. The (100), (002) and (101) planes appeared, which shows compatibility with the XRD results. The particle size diameters of the samples ranged from 5–30 nm, as presented in the particle size diameter distribution histograms in Fig. 3e and f.

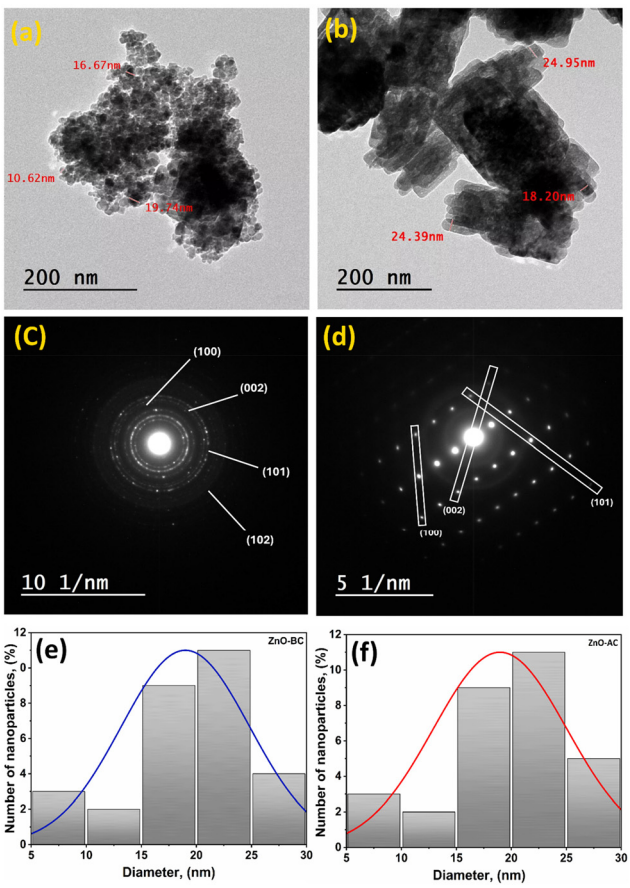

Fig. 3 (a and b) TEM Images for ZnO-BC and ZnO-AC, (c and d) SAED images of ZnO-BC and ZnO-AC, and (e and f) particle size diameter distribution histograms for ZnO-BC and ZnO-AC.

FT-IR spectroscopy. The FT-IR spectra of both ZnO-BC and ZnO-AC are presented in Fig. 4a. The ZnO-BC sample shows a peak at 3394 cm^{-1} indicating the stretching vibrations of water molecules. Furthermore, the peaks at 2997, 1647, 1481, and 1058 cm^{-1} were assigned to the stretching of C–H, C═O, C–H deformation, and stretching vibrations of C–O, respectively, originating from the remaining ASCBE extract used in the preparation process.[52] Additionally, the peaks at 585 and 458 cm^{-1} were attributed to Zn–O stretching vibrations.[53] These peaks nearly disappear in the ZnO-AC spectra due to the complete removal of the phytochemical groups. In the case of ZnO-AC, the peaks at 485 to 458 cm^{-1} showed defined splitting attributed to the purity and clear presence of ZnO-NPs. On the other hand, in the case of ZnO-BC, the peaks appearing from 485–458 cm^{-1} had an obvious shift to lower wavelength due to the presence of phytochemical groups.

UV-visible spectroscopic analysis. Fig. 4b shows the UV-visible absorption spectra for both ZnO-BC and ZnO-AC. Absorption peaks were observed at 360 and 372 nm for ZnO-BC and ZnO-AC, respectively.[54] A notable blue shift in the absorption spectrum of ZnO-BC to 360 nm compared to 372 nm for ZnO-AC was observed. This can be attributed to the conjugation bonds present in ASCBE within ZnO-BC. This conjugation enhanced the energy of the highest occupied molecular orbital and quenched or decreased the energy of the lowest unoccupied molecular orbital. Hence, less energy is needed for an electronic transition to occur in a conjugated system. As the number of conjugated bonds increases, the absorption peak value also increases. Increasing double bonds within the conjugation reduces the energy needed for electronic transitions. In addition, conjugation between two chromophores also increases molar absorptivity and intensity.[55] The energy band gap is illustrated in Fig. 4c. In the case of ZnO-AC, the energy band gap was decreased from 2.98 to 2.7 eV. This is due to the removal of organic compounds present in ASCBE, which led to higher absorption of energy.

PL spectra analysis. Fig. 4d presents the photoluminescence (PL) spectra of the ZnO-BC and ZnO-AC samples. The PL spectra of ZnO-BC exhibited an emission band observed at a wavelength of 392 nm, likely resulting from the band-to-band emission between the conduction band and valence band.[56–58] Furthermore, a broad visible emission band centred at 470 nm originates from structural defects such as zinc vacancies, oxygen vacancies, and lattice defects.[56] In the PL spectra of ZnO-AC, a blue shift of the UV emission band to 395 nm can

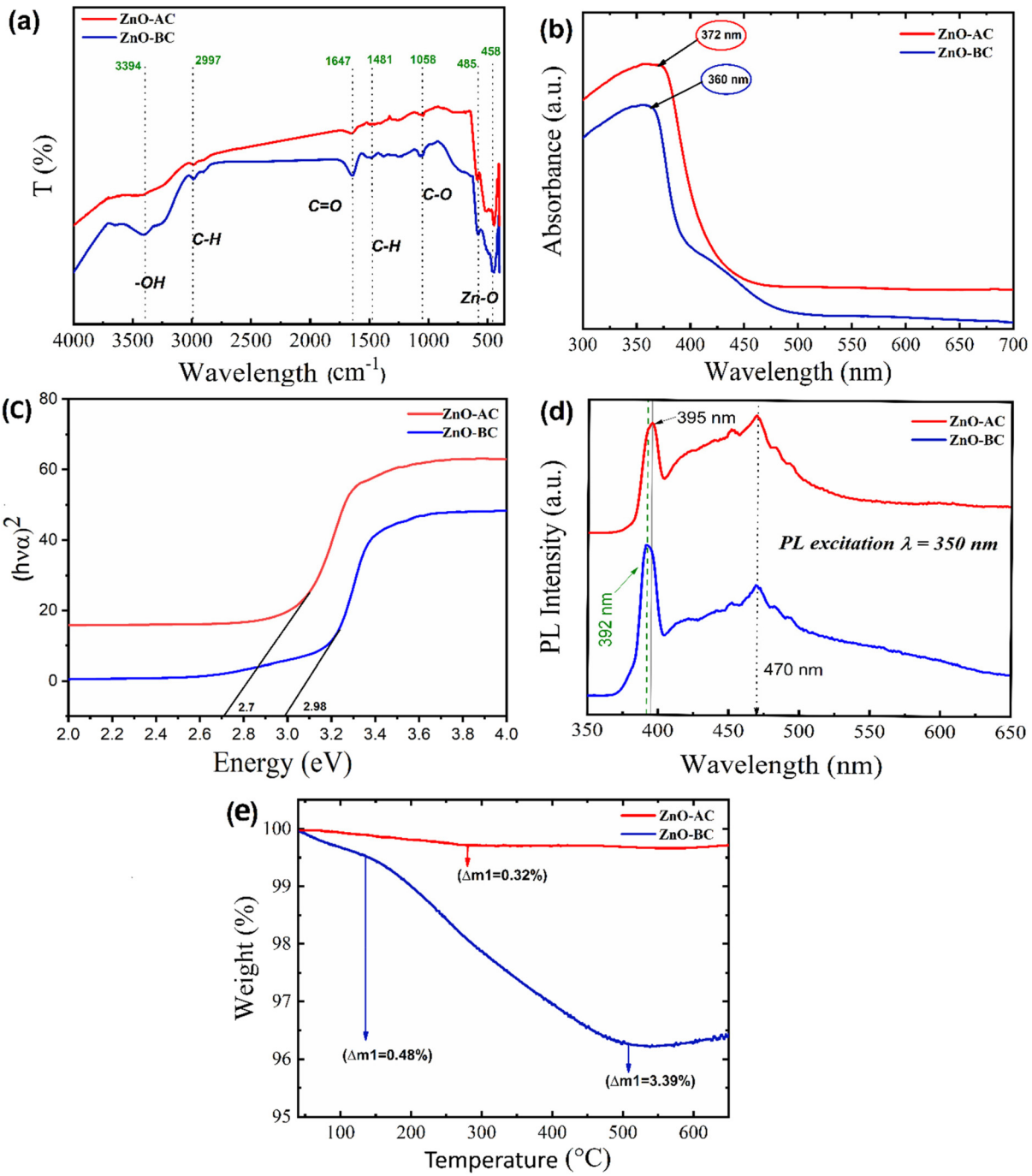

Fig. 4 (a) FT-IR spectra for ZnO-BC and ZnO-AC. (b) UV-visible spectra for ZnO-BC and ZnO-BC. (c) Band gap energy of ZnO-BC and ZnO-AC. (d) PL excitation spectra for ZnO-BC and ZnO-AC at 350 nm. (e) TGA of ZnO-BC and ZnO-AC.

be observed, accompanied by a decrease in intensity compared to ZnO-BC, which is attributed to the Stern–Volmer quenching effect.[59] On the other hand, the intensity of the visible emission peak became stronger due to thermal treatment, indicating an increase in defect levels.

TGA analysis. The thermal analysis of ZnO-BC and ZnO-AC samples was estimated to study their thermal stability and to determine the required temperature for the calcination step. The thermogram in Fig. 4e reveals that ZnO-BC underwent two distinct stages. The first stage exhibited a weight loss of 0.48% as the temperature rose to 134 °C, likely due to the evaporation of physically bonded water caused by hydrophilic phytochemicals responsible for water adsorption.[60] The second stage indicated a weight loss of 3.39% when heated up to 500 °C, which was attributed to the breakdown of the phytochemicals capping the ZnO-NPs. After 500 °C, the material remained

thermally stable, with no further weight loss. Additionally, the TGA of ZnO-AC showed a trace amount of sugarcane bagasse extract, about 0.32% of the total mass. The TGA result indicated that the average temperature required for the calcination of ZnO-BC to ZnO-AC is approximately 500 °C. The results also demonstrated that the proposed synthesis method of ZnO-NPs accomplished a high yield of 96.5%.

Proposed formation mechanism of ZnO-NPs mediated by aqueous sugarcane bagasse extract (ASCBE)

The formation mechanism was deduced based on experimental observations and characterization results of ASCBE and ZnO-NPs and relying on the fact that plant extracts usually work as antioxidant,[61] capping,[62] and stabilizing[63] agents. The formation of ZnO-NPs is divided into three major stages according to the role of ASCBE in each stage as shown in Fig. 5 and Fig. S1†-reaction schemes, as described below. (The luteolin molecule structure represents all phytochemical molecules, either phenolics or flavonoids, as it was reported to exist in bagasse extract.)[64]

Stage 1. Role of ASCBE as an antioxidant agent. The phytochemicals in ASCBE are water soluble mainly due to H-bonding formation,[65] as shown in Fig. 5a and Fig. S1†-reaction scheme (i). When zinc acetate dehydrate is added to the reaction medium in an excess amount compared to the extract, it dissociates into zinc and acetate ions, as shown in Fig. 5a and Fig. S1†-reaction scheme (ii). The antioxidant activity of phytochemicals can be found in a wide variety of actions; one of these actions is the chelation of transition metals, which is proposed to occur in this case. The presence of zinc ions motivates the ionization of phytochemicals, as represented in Fig. 5a and Fig. S1†-reaction scheme (iii).[66] The phytochemical ligand reduces some zinc ions to form a stable, uncharged complex, as seen in Fig. 5a and Fig. S1†-reaction

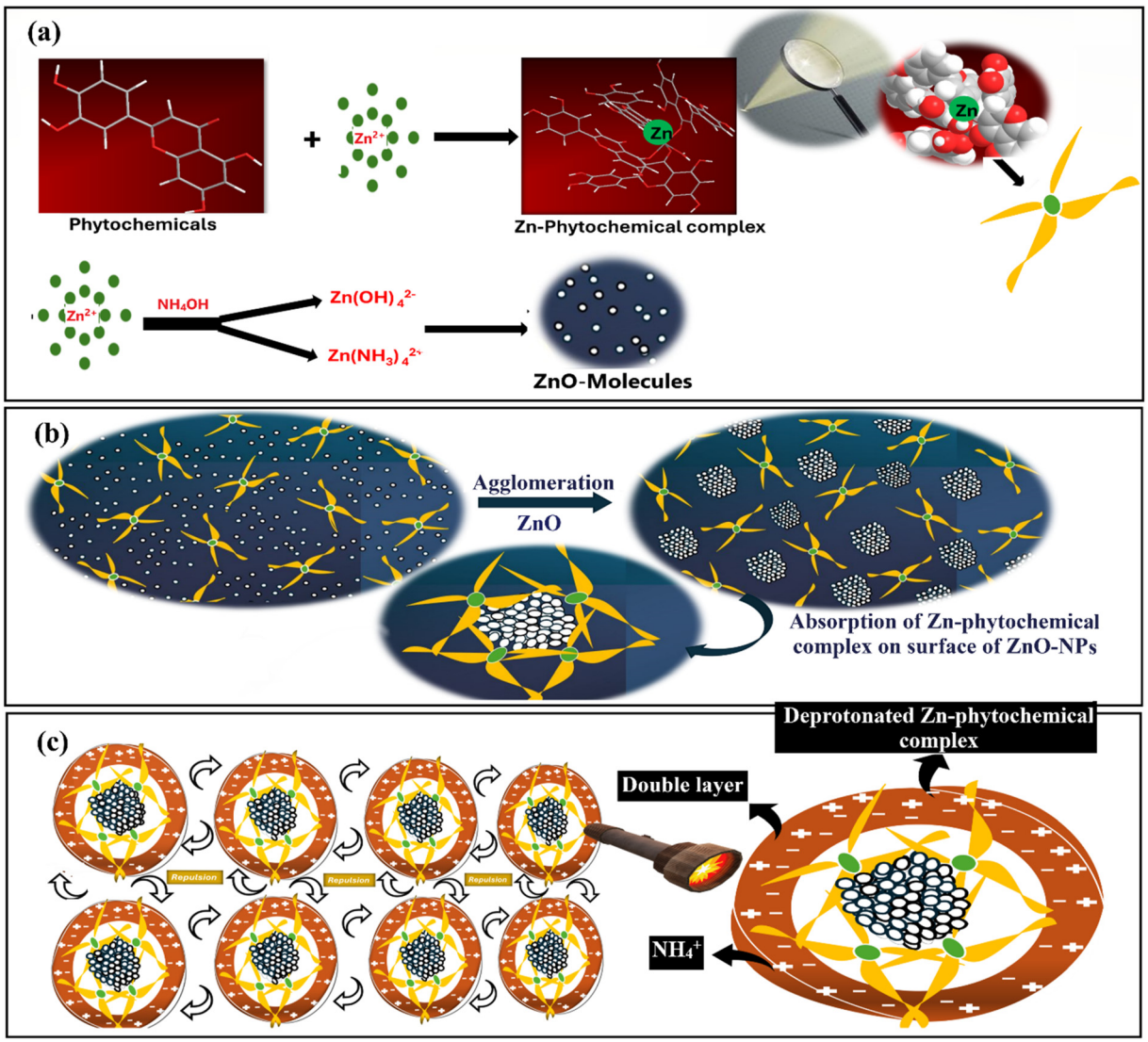

Fig. 5 The proposed formation mechanism of ZnO-NPs mediated by plant extract (sugarcane bagasse): (a) stage 1 – role of plant extract as antioxidant agent; (b) stage 2 – role of plant extract as capping agent; and (c) stage 3 – role of plant extract as stabilizing agent.

scheme (iv). At this point of the reaction, very small particle dots can be seen by the naked eye, as presented in Fig. 1f, due to the formation of a neutral complex. A concentrated solution of ammonia is added, which reacts with the remaining unreacted zinc ions. This will lead to the formation of tetraamine zincate ions, $[Zn(NH_3)_4]^{2-}$ and tetrahydroxozincate ions, $[Zn(OH)_4]^{2-}$,[67] which are unstable with an excess of hydroxide ions and upon raising the temperature are broken down to form ZnO molecules, as shown in Fig. 5a and Fig. S1†-reaction scheme (v).

Stage 2. Role of ASCBE as capping agent. ZnO molecules tend to agglomerate with one another to form NPs, as shown in Fig. 5b. Additionally, the addition of ammonia makes the solution basic, which causes the deprotonation of phytochemicals and leads to the formation of negative charges on the zinc–phytochemical complex, as shown in Fig. 5b and Fig. S1†-reaction scheme (vi); this effect can be reversed by the removal of ammonia. The presence of Zn–phytochemicals all throughout the solution disables further agglomeration of ZnO molecules, turning into a large precipitate. According to adsorption laws, particles tend to be adsorbed on surfaces that have the same ion species, *i.e.*, the charged zinc–phytochemical complex is adsorbed on the surface of the formed ZnO-NPs gradually until it fully caps the NPs, which prevents further crystal growth of the ZnO-NPs, as represented in Fig. 5b.

Stage 3. Role of ASCBE as stabilizing agent. Fig. 5c represents the stabilization stage of the ZnO-NPs. The zinc–phytochemical complex spheres remain negatively charged as long as ammonia is still in solution, which causes the repulsion of NPs capped with charged complexes, preventing the settling of the ZnO-NPs, as shown in Fig. 1h. All ammonia is removed through continuous heating to collect the ZnO nanoparticles.

Biological activity

Antimicrobial assessment of ZnO-BC and ZnO-AC. The green-synthesized ZnO-NPs exhibited stronger antimicrobial activity against both *P. aeruginosa* and *A. niger* compared to the calcined ZnO-NPs. The green-synthesized ZnO-NPs showed inhibition zones of 34.25 ± 0.52 mm and 22.45 ± 0.47 mm for *P. aeruginosa* and *A. niger*, respectively, while the calcined ZnO-NPs showed inhibition zones of 17.19 ± 0.13 mm and 15.57 ± 0.41 mm for the same pathogens (Fig. 6). The enhanced antimicrobial activity of ZnO-BC compared to ZnO-AC could be attributed to the phytochemical constituents, such as phenolics and flavonoids, present in the ASCBE used for the green synthesis. During the green synthesis process, these capping ZnO-NPs enhance antimicrobial properties.[68] The antioxidant and free radical scavenging activity of the phytochemicals could have contributed to the improved antimicrobial efficacy of ZnO-BC against the tested pathogens, *P. aeruginosa* and *A. niger*,[69] because it imparted its properties with the nanoparticles. In contrast, the calcination process used to obtain ZnO-AC caused the removal of the phytochemical properties, potentially reducing their antimicrobial activity and diminishing the synergistic antimicrobial effects observed in ZnO-BC.[70] The results suggest that the green synthesis approach utilizing ASCBE as a reducing and capping agent is more effective for producing ZnO-NPs with enhanced antimicrobial properties than the traditional calcination method. Integrating the bioactive phytochemicals from sugarcane bagasse into the ZnO-NPs during the green synthesis process appears to be a critical factor in the improved antimicrobial efficacy of the green-synthesized ZnO-NPs.

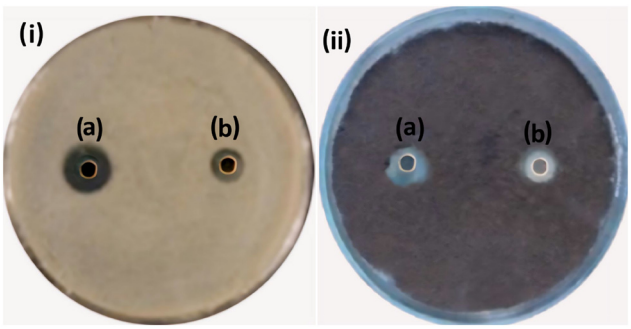

Fig. 6 Antimicrobial activity of: (a) ZnO-BC and (b) ZnO-AC against (i) *P. Aeruginosa* ATCC 27853, and (ii) *A. Niger* ATCC 16888.

Molecular docking of ZnONPs against microbial and viral targets. The molecular docking results showed that the ZnO-NPs exhibited the strongest binding affinity towards the *P. aeruginosa* RhlG/NADP active-site complex, with a MolDoc score of −41.282 and four hydrogen bond interactions with key amino acid residues (Ala 167(A), His 170(A), Gln 172(A) and Gly 151(B)). The ZnO-NPs also showed promising binding interactions with the crystal structure of Actibind, a T2 RNase of *A. niger*, with a MolDoc score of −25.292 and three hydrogen bond interactions (Tyr 62, Tyr 200, and Glu 221). For the Herpes simplex virus type II protease, a DNA virus, the ZnO-NPs displayed a MolDoc score of −15.407 with two hydrogen bond interactions (Ala 217(A) and Asn 220(A)). The ZnO nanoparticles also interacted with the Influenza virus NS1 effector domain, an RNA virus, with a MolDoc score of −20.328 and two hydrogen bond interactions (Leu 90 (A) and Arg 200 (B)) (Fig. 7). Molecular docking results suggest that the ZnO-NPs have the potential to interact with and potentially inhibit the functions of both microbial and viral targets. The stronger binding affinities observed towards the microbial targets, *P. aeruginosa* RhlG/NADP active-site complex and Actibind (a T2 RNase of *A. niger*), indicate that the ZnO-NPs could be more effective in inhibiting these microbial enzymes. The high MolDoc score (−41.282) and the four hydrogen bond interactions between the ZnO-NPs and the *P. aeruginosa* RhlG/NADP active-site complex suggest a strong binding affinity. The RhlG enzyme is crucial for quorum sensing and virulence regulation in *P. aeruginosa*.

By disrupting the RhlG function, the ZnO-NPs could potentially contribute to the inhibition of *P. aeruginosa* growth and pathogenicity. Similarly, the promising binding interactions of the ZnO-NPs with the crystal structure of Actibind, a T2 RNase of *A. niger* (MolDoc score of −25.292 and three hydrogen bond interactions), indicate the potential of the ZnO-NPs to inhibit the RNase activity of Actibind. This could have implications

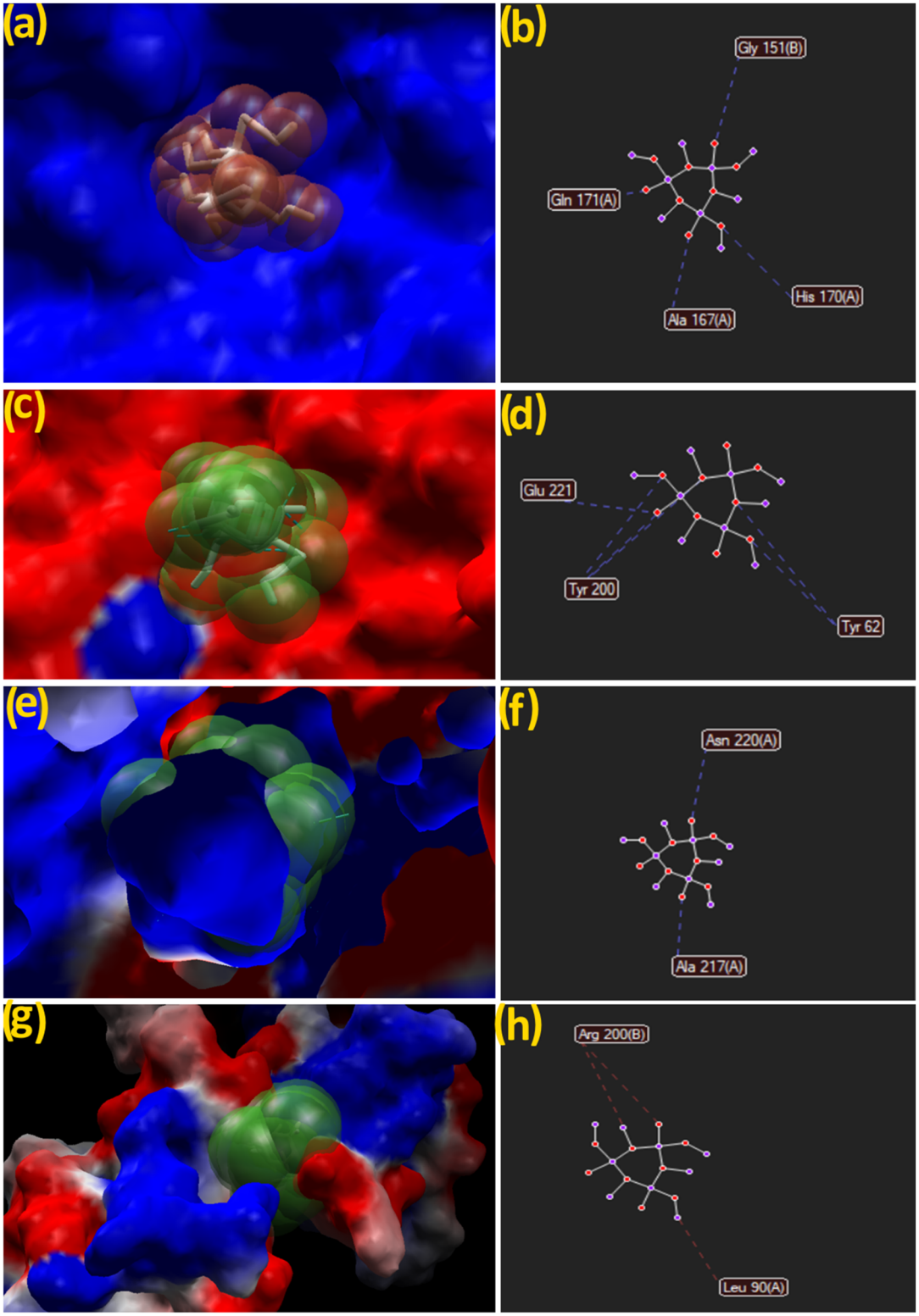

Fig. 7 Binding interactions of ZnO-NPs: (a and b) *P. Aeruginosa* RhlG/NADP active-site complex, (c and d) crystal structure of ACTi binding a T2 RNase of *A. Niger*, (e and f) herpes simplex virus type II protease and (g and h) influenza virus NS1 effector domain protein.

for the development of ZnO-NPs-based antifungal agents targeting *A. niger* and other fungal pathogens. The stronger binding affinities of the ZnO-NPs towards the microbial targets suggest that they could be more effective as antimicrobial agents than as antiviral agents. The identified hydrogen bond interactions with the viral targets, herpes simplex virus type II

protease, and influenza virus NS1 effector domain provide insights into the potential interaction mechanisms between the ZnO-NPs and these viral proteins. The findings of the molecular docking study indicate that ZnO-NPs have the potential to be developed as antimicrobial agents, particularly targeting *P. aeruginosa* and *A. niger*. The stronger binding affinities observed towards the microbial targets suggest that the ZnO-NPs could be more effective in inhibiting the functions of these microbial and viral active sites.[71] Green ZnO-NPs were synthesized using *Dysphania ambrosioides* extract, and their antimicrobial activity against various pathogenic bacteria was evaluated. The NPs, ranging from 7 to 130 nm, were formed at varying reaction temperatures from 200 to 800 °C. The study found that smaller ZnO-NPs showed higher inhibition against Gram-positive and Gram-negative bacteria and oral pathogens. The molecular docking analysis suggested potential interactions between ZnO-NPs and bacterial proteins like TagF in *Staphylococcus epidermidis* and AcrAB-TolC in *E. coli*. This study provides insights into how the physicochemical properties of green-synthesized ZnO-NPs, particularly their size, influence their antimicrobial efficacy against various pathogenic bacteria. Additionally, their antiviral activity was evaluated against human coronavirus 229E. The ZnO-NPs with an average size of 12.1 nm were found to have enhanced antiviral activity when combined with the plant extract. The *C. diurnum* leaf extract and the ZnO-NPs showed antiviral activity against HCoV-229E, but their combination showed higher activity. The molecular docking results suggest that phytochemicals from *C. diurnum* can directly target key viral proteins, such as the main protease of HCoV-229E.

Economic and environmental studies. As referred to in our research work, scientific studies cannot be separated from real life, as represented by environmental, materialistic, energetic, time, and human resource factors. Thus, economic research was done to evaluate the materials consumption required to obtain 1 kg of green-synthesized, pure, highly crystalline ZnO-NPs with an average particle size of 5–30 nm. The amount of agricultural industrial waste that can be beneficial in green synthesis was investigated. The quantitative analysis of the raw materials required to obtain 1 kg of ZnO-AC was executed and is presented in Table 2, based on the fact that the amount of ZnO-AC produced is about 96.5% that before calcination. As presented in Table 2, about 5 kg of dried sugarcane bagasse is needed to produce 1 kg of ZnO-AC. It was worth studying how much waste we can eliminate or minimize from our environment. In addition, free and clean space can be provided after minimizing the waste amount throughout the whole process of the formation of 1 kg ZnO-AC as presented in Table 3, based on the fact that dried sugarcane bagasse occupies about 60% of the volume of fresh sugarcane bagasse. Moreover, the volume occupied by sugarcane bagasse waste was reduced from 0.375 m^3 to 0.008 m^3, which would be more easily disposed of. Additionally, the residual sugarcane bagasse fibers have high potential in many applications including the paper industry, as feedstocks, and as a biofuel.[72] They can also be used in the fabrication of fibrous thermal insulation and sound absorbers,[73] especially in the form they gained throughout the extraction process, which is in accordance with sustainability principles.

Table 4 compares different plants used for the green synthesis of ZnO-NPs and the resultant shape, size and antibacter-

Table 2 Proposed study of the amounts of raw materials required for preparing 1 kg of pure ZnO-NPs

Items	Dried sugarcane bagasse (g)	Extract crystals (g)	Zinc acetate precursor (g)	ZnO-BC (g)	ZnO-AC (g)
Standard quantity	100	14	70	21	20.16
Quantity for 1 kg of ZnO-AC	4960	695	3475	1041	1000

Table 3 Environmental study of waste minimization resulting from preparing 1 kg of ZnO-NPs

Dried sugarcane bagasse (kg)	Fresh sugarcane bagasse (kg)	Residual sugarcane bagasse after extraction (kg)	Volume occupied by fresh sugarcane bagasse (m^3)	Volume occupied by residual sugarcane bagasse (m^3)
5	8.33	3.55	0.375	0.008

Table 4 Different plants used for green synthesis of ZnO-NPs and resultant shape, size, and antibacterial activity of nanoparticles

Plant	Shape	Particle size diameter (nm)	Antibacterial activity inhibition zone (mm) *P. aeruginosa*	Ref.
Pelargonium odoratissimum	Hexagonal-like	34.1	21 mm	74
Ocimum basilicum	Heterogeneous	18–30	25 mm	75
Pongamia pinnata	Rod	200	19 mm	76
Veronica multifida	Hexagonal and quasi-spherical	10–100	9 mm	77
Sugarcane bagasse	Hexagonal-like	5–30	34 mm	This work

ial activity of the nanoparticles. The data reveals that our green-synthesized ZnO-NPs (ZnO-BC) have the largest inhibition zone among all the materials for the same type of bacteria and the smallest particle size.

Experimental

Materials and reagents

50 kg of sugarcane bagasse waste was supplied from Egyptian Sugar and Integrated Industries CO. ESIIC, El Hawamdeya, Giza, Egypt. Zinc acetate dehydrated (98% purity) was purchased from El-gomhouria chemical company, Cairo, Egypt. Ammonia hydroxide (98% purity), and ethanol (95% purity) were purchased from Merck. All chemicals were used without purification.

Preparation of aqueous sugarcane bagasse extract (ASCBE)

The sugarcane bagasse waste was cleaned carefully using distilled water to remove any impurities and/or dust. It was then sun-dried for approximately one week. Subsequently, it was milled until it turned into powder and small fibers. 100 g of the milled plant was boiled in double-distilled water (DDW) for 2 hours. The mixture was filtered using Whatman No. 1 filter paper to separate the filtrate (extract) from plant residuals. The filtrate was concentrated into a solid extract powder using a Heidolph rotary evaporator overnight for yield estimation and easy storage purposes. Fig. 1 shows the sequential stages of obtaining the concentrated solid powder of ASCBE.

Phytochemical analysis of ASCBE

See the ESI† for details.

Green synthesis of ZnO-NPs

4.0 g of the solid sugarcane bagasse solid extract crystals were dissolved in 1.0 L of double-distilled water. Next, 20.0 g of zinc acetate was dissolved in the extract solution. The mixture was heated on a direct flame until it boiled for about 20 min. A few drops of concentrated ammonium hydroxide were then added until ZnO-NPs appeared. Afterward, the ZnO-NPs were collected and rinsed multiple times with double-distilled water and 95% ethanol, then left to air-dry for three days to produce ZnO-BC. Finally, the resulting powder was calcined at 550 °C, 2 °C min^{-1} for 2 h to obtain pure ZnO-AC.[78]

Characterization techniques

See the ESI† for details.

Biological activity study

Antimicrobial evaluation of the green-synthesized ZnO-nanoparticles (ZnO-BC) and calcined ZnO nanoparticles (ZnO-AC) was conducted. Both ZnO-BC and ZnO-AC were tested for their antibacterial and antifungal activity using the well diffusion method.[79] The selected pathogens were *Pseudomonas aeruginosa* ATCC 27853 and *Aspergillus niger* ATCC 16888. For each pathogen, 30 μg ml^{-1} of the ZnO nanoparticles were inoculated into a 5 mm well in the seeded agar plates.

Molecular docking

The molecular docking of ZnO-NPs was performed against the following targets obtained from the protein data bank (PDB) using the Molegro Virtual Docker software: *P. aeruginosa* RhlG/NADP active-site complex (PDB: 2b4q), crystal structure of Actibind, a T2 RNase of *A. niger* (PDB: 3d3z), Herpes simplex virus type II protease (PDB: 1at3), a DNA virus, and Influenza virus NS1 effector domain (PDB: 2gx9), an RNA virus. The ZnO-NPs were drawn using Material Studio.[80]

Conclusions

It can be concluded that the industrial waste sugarcane bagasse has high potential in the green synthesis field, and that it is a very suitable medium for the fabrication of ZnO-NPs. A series of comparisons between ZnO-BC and ZnO-AC achieved the main goal of this study, which was sustainability not only in reusing waste but also in finding ways of saving energy. XRD revealed that both samples have a zincite phase with a negligible shift in the 2θ angle of about 0.019° in ZnO-BC. TEM images showed that ZnO-BC had a smaller size and more dispersed particles due to the presence of a capping agent. FT-IR spectra for both samples indicated the presence of some functional groups ascribed to the presence of ASCBE in the ZnO-BC sample, but in ZnO-AC, these nearly disappeared due to the removal of most of the ASCBE in the calcination step. UV absorption spectra showed a shift in the ZnO-BC spectrum; the maximum absorption wavelength was 372 nm, while that of ZnO-AC was 360 nm. The TGA results showed that the un-calcined ZnO-NPs contained about 4% of physically bonded water and ASCBE residues, which was considered to indicate a relatively very high yield of ZnO-NPs. On the other hand, ZnO-AC contained about 0.32% of impurities. Phytochemical assessment of ASCBE showed it has phenolics, flavonoids and antioxidant activity, enabling it to act as a reducing agent for the zinc precursor. The findings of this study suggest that the green-synthesized ZnO-NPs exhibit enhanced antimicrobial activity compared to the calcined ZnO-NPs, likely due to the incorporation of beneficial phytochemicals from the sugar beet used in the green synthesis process. The stronger binding affinities of the ZnO-NPs towards the microbial targets, particularly the *P. aeruginosa* RhlG/NADP active-site complex and the crystal structure of Actibind from *A. niger*, indicate their potential as effective antimicrobial agents. The molecular docking results also provide insights into the potential interactions between the ZnO-NPs and viral targets, such as the Herpes simplex virus type II protease and Influenza virus NS1 effector domain. The proposed mechanism for forming ZnO-NPs mediated by ASCBE was studied, and the important role of ASCBE was explained. Finally, environmental and economic studies were conducted to relate our study to the reality of daily life. The results demonstrated

that the calcination step is a step that can be dispensed with, and that there were not substantial differences between ZnO-BC and ZnO-AC. Moreover, the fabrication of ZnO-NPs using this method reduces energy consumption and leads to higher biological activity.

Data availability

All data generated or analysed during this study are included in this published article [and its ESI†].

Conflicts of interest

There are no conflicts to declare.

Acknowledgements

This work was supported by the financial support of the Science and Technology Development Fund (STDF) Foundation of the Project No. (37068).

References

1 E. Kianfar, *Importance Appl. Nanotechnol.*, 2020, vol. 5, pp. 22–25.
2 V. M. Rodriguez and H. A. Abhyankar, *Nanocomposite Materials*, CRC Press, London, 1st edn, 2016, pp. 81–103.
3 G. E. Yılmaz, I. Göktürk, M. Ovezova, F. Yılmaz, S. Kılıç and A. Denizli, *Hygiene*, 2023, **3**, 269–290.
4 J. Nandhini, E. Karthikeyan and S. Rajeshkumar, *Biomed. Technol.*, 2024, **6**, 26–45.
5 J. I. Koga, T. Matoba and K. Egashira, *J. Atheroscler. Thromb.*, 2016, **23**, 757–765.
6 S. Kulkarni and A. K. H. Sonali, *Novel Technologies in Biosystems, Biomedical & Drug Delivery*, Springer Nature, Singapore, 2023.
7 A. Singh, P. Rajput, R. Chopra, Ankush, S. Singh, A. Singh and P. Singh, *Microbial Synthesis of Nanomaterials*, Nova Science Publishers, Inc., New York, 2021, pp. 163–177.
8 M. M. Khin, A. S. Nair, V. J. Babu, R. Murugan and S. Ramakrishna, *Energy Environ. Sci.*, 2012, **5**, 8075–8109.
9 M. Z. Al Mahmud, *J. Nanomater.*, 2023, **2023**, 5432099.
10 M. H. V. Mhetre, D. Y. K. Kanse and D. S. S. Patil, *Int. J. Adv. Eng. Nano Technol.*, 2021, **4**, 7–19.
11 D. G. Tamrakar and S. S. Thakur, *Migr. Lett.*, 2023, **20**, 1–18.
12 P. Jangid and M. P. Inbaraj, *Mater. Today Proc.*, 2021, **43**, 2877–2881.
13 L. M. Pandey and A. Hasan, *Nanoscale Engineering of Biomaterials: Properties and Applications*, Springer Nature, Singapore, 2022.
14 S. M. Sheta and S. M. El-Sheikh, *Anal. Biochem.*, 2022, **648**, 114680.
15 S. M. Sheta, S. R. Salem and S. M. El Sheikh, *J. Mater. Res.*, 2022, **37**, 2356–2367.
16 A. S. Basaleh and S. M. Sheta, *Anal. Bioanal. Chem.*, 2020, **412**, 3153–3165.
17 S. M. Sheta, S. M. El-Sheikh and M. M. Abd-Elzaher, *Dalton Trans.*, 2018, **47**, 4847–4855.
18 S. Ying, Z. Guan, P. C. Ofoegbu, P. Clubb, C. Rico, F. He and J. Hong, *Environ. Technol. Innovation*, 2022, **26**, 102336.
19 I. H. Ifijen, M. Maliki and B. Anegbe, *OpenNano*, 2022, **8**, 100082.
20 A. Singh, P. Tyagi, R. Ranjan, S. N. Sushkova, T. Minkina, M. Burachevskaya and V. D. Rajput, *Processes*, 2023, **11**, 141.
21 D. D. Suppiah, N. M. Julkapli, S. Sagadevan and M. R. Johan, *Inorg. Chem. Commun.*, 2023, **152**, 110700.
22 H. M. Abuzeid, C. M. Julien, L. Zhu and A. M. Hashem, *Crystals*, 2023, **13**, 1576.
23 A. I. Osman, Y. Zhang, M. Farghali, A. K. Rashwan, A. S. Eltaweil, E. M. Abd El-Monaem, I. M. A. Mohamed, M. M. Badr, I. Ihara, D. W. Rooney and P. S. Yap, *Environ. Chem. Lett.*, 2024, **22**, 841–887.
24 P. V. Megha, K. B. Joseph and X. Mohanan, *Biomedical Applications and Toxicity of Nanomaterials*, Springer Nature, Singapore, 2023, pp. 319–338.
25 N. M. Shinde, A. C. Lokhande and C. D. Lokhande, *J. Photochem. Photobiol., B*, 2014, **136**, 19–25.
26 G. F. Perotti and L. P. da Costa, in *Reducing Agents in Colloidal Nanoparticle Synthesis*, ed. S. Mourdikoudis, The Royal Society of Chemistry, 2021, pp. 316–332.
27 R. Álvarez-Chimal and J. Ángel Arenas-Alatorre, *Green Synthesis of Nanoparticles: A Biological Approach*, IntechOpen, UK, 2023.
28 Y. Zhang, Y. R. Leu, R. J. Aitken and M. Riediker, *Int. J. Environ. Res. Public Health*, 2015, **12**, 8717–8743.
29 F. Piccinno, F. Gottschalk, S. Seeger and B. Nowack, *J. Nanopart. Res.*, 2012, **14**, 1109.
30 N. González, M. Del Àngels Custal, D. Rodríguez, J. R. Riba and E. Armelin, *Mater. Res.*, 2017, **20**, 1082–1091.
31 E. E. Elemike, I. M. Uzoh, D. C. Onwudiwe and O. O. Babalola, *Appl. Sci.*, 2019, **9**, 499.
32 K. Srinivas, *Int. J. TechnoChem Res.*, 2018, **04**, 27–39.
33 K. Ghule, A. V. Ghule, B. J. Chen and Y. C. Ling, *Green Chem.*, 2006, **8**, 1034–1041.
34 C. Liu, C. Xiao and W. Li, *J. Mater. Chem. C*, 2021, **9**, 14093–14114.
35 R. F. Zhuo, L. Qiao, H. T. Feng, J. T. Chen, D. Yan, Z. G. Wu and P. X. Yan, *J. Appl. Phys.*, 2008, **104**, 094101.
36 Ü. Ozgur, D. Hofstetter and H. Morkoç, *Proc. IEEE*, 2010, **98**, 1255–1268.
37 J. Jiang, J. Pi and J. Cai, *Bioinorg. Chem. Appl.*, 2018, **2018**, 1–18.
38 D.-S. Guo, G.-H. Chen, M.-Z. Tong, C.-Q. Wu, R. Fang and L.-X. Yi, *Chin. J. Anal. Chem.*, 2012, **40**, 72.
39 F. Z. Bedia, A. Bedia, B. Benyoucef and S. Hamzaoui, *Phys. Procedia*, 2014, **55**, 61–67.
40 J. Pan, J. Chen, Q. Huang, Q. Khan, X. Liu, Z. Tao, W. Lei, F. Xu and Z. Zhang, *RSC Adv.*, 2015, **5**, 82192–82198.
41 A. B. Mousa, R. Moawad, Y. Abdallah, M. Abdel-Rasheed and A. M. A. Zaher, *Pharm. Res.*, 2023, **40**, 2281–2290.

42 C. Wu, T. Zhang, B. Ji, Y. Chou and X. Du, *Cellulose*, 2024, **31**, 4849–4864.
43 M. M. Chikkanna, S. E. Neelagund and K. K. Rajashekarappa, *SN Appl. Sci.*, 2019, **1**, 117.
44 N. Rani, S. Yadav, A. Mushtaq, S. Rani, M. Saini, S. Rawat, K. Gupta, K. Saini and D. Maity, *Chem. Pap.*, 2024, **78**, 3687–3704.
45 B. Gajdzik, R. Wolniak, R. Nagaj, B. Žuromskaitė-Nagaj and W. W. Grebski, *Energies*, 2024, **17**, 947.
46 I. Khalid, S. Ullah and I. S. Umar, *Int. J. Adv. Sci. Comput. Appl.*, 2021, **1**, 27–40.
47 J. Kim, *IMF Work. Pap.*, 2024, **2024**, 1.
48 M. A. Mahmud and F. R. Anannya, *Heliyon*, 2021, **7**, e07771.
49 K. A. Akinkuade, I. P. Olasesan, O. A. Fakayode, A. A. Odesanmi and O. A. Ajibade, *World News Nat. Sci.*, 2022, **45**, 117–142.
50 A. A. Azmi and S. A. Othman, *AIP Conf. Proc.*, 2023, **2544**, 040034.
51 H. Rashidi, A. Ahmadpour, F. F. Bamoharram, S. M. Zebarjad, M. M. Heravi and F. Tayari, *Chem. Pap.*, 2014, **68**, 516–524.
52 S. Azizi, R. Mohamad, R. A. Rahim, A. B. Moghaddam, M. Moniri, A. Ariff, W. Z. Saad and F. Namvab, *Appl. Surf. Sci.*, 2016, **384**, 517–524.
53 M. L. da Silva-Neto, M. C. A. de Oliveira, C. T. Dominguez, R. E. M. Lins, N. Rakov, C. B. de Araújo, L. de S. Menezes, H. P. de Oliveira and A. S. L. Gomes, *Sci. Rep.*, 2019, **9**, 11765.
54 S. Pehlivanoglu, C. A. Acar and S. Donmez, *Inorg. Nano-Met. Chem.*, 2021, **53**, 1022–1031.
55 F. A. Carey, *Org. Chem. Front.*, 2022, **1261**, 1261.
56 V. Chandrasekaran, S. Chidambaram and M. K. Ganesan, *J. Mater. Sci.: Mater. Electron.*, 2018, **29**, 667–673.
57 S. Annathurai, S. Chidambaram, B. Baskaran and G. K. D. Prasanna Venkatesan, *J. Inorg. Organomet. Polym. Mater.*, 2019, **29**, 535–540.
58 D. Shao, M. Yu, H. Sun, T. Hu, J. Lian and S. Sawyer, *Nanoscale*, 2013, **5**, 3664–3667.
59 V. Subramanian, E. E. Wolf and P. V. Kamat, *J. Phys. Chem. B*, 2003, **107**, 7479–7485.
60 P. Delmondes and R. Stefani, MOL2NET'16, Conference on Molecular, Biomed., Comput. & Network Science and Engineering, 2nd edn, 2022, MOL2NET: FROM MOLECULES TO NETWORKS, 15–20 Oct 2022.
61 M. J. Rodríguez-Yoldi, *Antioxidants*, 2021, **10**, 921.
62 M. A. Betiha, Z. M. Kheiralla, A. S. Mansour, A. N. Emam, S. B. El-Henawy, E. A. Mohamed and N. A. Negm, *Egypt. J. Chem.*, 2022, **65**, 575–589.
63 Z. Villagrán, L. M. Anaya-Esparza, C. A. Velázquez-Carriles, J. M. Silva-Jara, J. M. Ruvalcaba-Gómez, E. F. Aurora-Vigo, E. Rodríguez-Lafitte, N. Rodríguez-Barajas, I. Balderas-León and F. Martínez-Esquivias, *Resources*, 2024, **13**, 70.
64 M. J. Houghton, R. J. S. Costa, B. Kitchen and G. Williamson, *Compr. Rev. Food Sci. Food Saf.*, 2024, **23**, e13307.
65 S. Rajhard, L. Hladnik, F. A. Vicente, S. Srčič, M. Grilc and B. Likozar, *Processes*, 2021, **9**, 1952.
66 A. Galano, *J. Mex. Chem. Soc.*, 2015, **59**, 231–262.
67 M. T. Thein, S. Y. Pung, A. Aziz and M. Itoh, *J. Exp. Nanosci.*, 2015, **10**, 1068–1081.
68 W. Ahmad and D. Kalra, *J. King Saud Univ., Sci.*, 2020, **32**, 2358–2364.
69 K. V. Dhandapani, D. Anbumani, A. D. Gandhi, P. Annamalai, B. S. Muthuvenkatachalam, P. Kavitha and B. Ranganathan, *Biocatal. Agric. Biotechnol.*, 2020, **24**, 101517.
70 A. Sangeetha, S. Jaya Seeli, K. P. Bhuvana, M. A. Kader and S. K. Nayak, *J. Sol-Gel Sci. Technol.*, 2019, **91**, 261–272.
71 R. Álvarez-Chimal, V. I. García-Pérez, M. A. Álvarez-Pérez, R. Tavera-Hernández, L. Reyes-Carmona, M. Martínez-Hernández and J.Á Arenas-Alatorre, *Arabian J. Chem.*, 2022, **15**, 103804.
72 L. Shu, C. C. Berndt and A. Hodzic, Proc ACUN-5 Developments Compos. Adv. Infrastructural, Nat. Nano-Composites, 2006, 11, 248–253.
73 S. Mehrzad, E. Taban, P. Soltani, S. E. Samaei and A. Khavanin, *Build. Environ.*, 2022, **211**, 108753.
74 A. S. Abdelbaky, T. A. Abd El-Mageed, A. O. Babalghith, S. Selim and A. M. H. A. Mohamed, *Antioxidants*, 2022, **11**, 1444.
75 Z. Ali and M. H. Risan, *J. Biotechnol. Res. Cent.*, 2024, **18**, 5–16.
76 M. Ghosh, V. U. Nallal, K. Prabha, S. Muthupandi and M. Razia, *Mater. Today Proc.*, 2021, **49**, 2632–2635.
77 S.Ş Doğan and A. Kocabaş, *Hum. Exp. Toxicol.*, 2020, **39**, 319–327.
78 I. N. Alrabayah, S. S. Elhawary, Z. A. Kandil, E. M. A. El-Kadder, Y. S. Moemen, A. M. Saleh and M. A. El Raey, *Molecules*, 2022, **28**, 266.
79 Z. Obeizi, H. Benbouzid, S. Ouchenane, D. Yılmaz, M. Culha and M. Bououdina, *Mater. Today Commun.*, 2020, **25**, 101553.
80 M. Ahmadi, A. Elikaei and P. Ghadam, *Iran. J. Microbiol.*, 2023, **15**, 138–148.